Corresponding Author: Dr. Pedro J. Fito, Dr. in Food Engineering

Corresponding Author's Institution: Universidad Politecnica de Valencia

First Author: Maria Victoria Traffano-Schiffo

Order of Authors: Maria Victoria Traffano-Schiffo; Marta Castro-Giraldez; Vicente Herrero; Ricardo J. Colom; Pedro J. Fito, Dr. in Food Engineering

Abstract: The trend in meat consumption has changed drastically in the last years, mainly due to the relationship of red and processed meats with cancer and cardiovascular diseases, which has caused a substantial growth in poultry meat consumption, 8% in 2016. Therefore, poultry production has suffered an intensification that has led to an increase in the incidence of internal malformations in chickens and turkeys for fattening, especially in the pectoral muscles, as Deep Pectoral Myopathy (DPM). Currently, industry is not able to detect DPM breasts when sold as whole carcasses. In this context, the use of dielectric spectroscopy, complemented by a deep study of the chemical, biochemical and microstructural transformations of the muscle and the effect that these changes have on the electrical dispersions in radiofrequency range, may become feasible for online DPM detection. For this paper, non-damaged and affected by DPM chicken breasts (pectoralis major and pectoralis minor) was analysed. Permittivity in radiofrequency and microwave ranges were measured in the different tissues: pectoralis minor, major and skin in order to characterize them. Moreover, proteins content, ion content and pH were measured. With this data, a sensor for measuring the permittivity of chicken whole carcass with skin was developed; it consists of two pairs of two flat plates sensor connected to an impedance Agilent analyzer 4294A and can measure the permittivity from 40 Hz to 1 MHz. The results demonstrated the feasibility of the permittivity in radiofrequency range as an identification technique of chicken breasts affected by DPM.

Highlights

> A deep microstructural study of normal and DPM chicken meat has been carried out

> Lactate content of each category has been related to the ε'_α

> The relation of proteins content of each category with the ε'_β has been obtained

> Dielectric properties of normal and DPM poultry meat were obtained in RF and MW ranges

> A non-destructive sensor able to detect DPM in whole carcasses has been developed

1 **DEVELOPMENT OF A NON-DESTRUCTIVE DETECTION SYSTEM OF**

2 **DEEP PECTORAL MYOPATHY IN POULTRY BY DIELECTRIC**

3 **SPECTROSCOPY**

4 **Maria Victoria Traffano-Schiffo[a], Marta Castro-Giraldez[a], Vicente Herrero[b];**

5 **Ricardo J. Colom[b]; Pedro J. Fito[a*]**

6 [a]Instituto Universitario de Ingeniería de Alimentos para el Desarrollo, Universitat

7 Politècnica de València, Camino de Vera s/n, 46022 Valencia, Spain.

8 [b]Instituto de Instrumentación para Imagen Molecular, Universitat Politècnica de

9 València, Camino de Vera s/n, 46022 Valencia, Spain.

10 *Corresponding author. Tel: +34 96 387 98 32

11 E-mail address: pedfisu@tal.upv.es

12 **ABSTRACT**

13 The trend in meat consumption has changed drastically in the last years, mainly due to

14 the relationship of red and processed meats with cancer and cardiovascular diseases,

15 which has caused a substantial growth in poultry meat consumption, 8% in 2016.

16 Therefore, poultry production has suffered an intensification that has led to an increase

17 in the incidence of internal malformations in chickens and turkeys for fattening,

18 especially in the pectoral muscles, as Deep Pectoral Myopathy (DPM). Currently,

19 industry is not able to detect DPM breasts when sold as whole carcasses. In this context,

20 the use of dielectric spectroscopy, complemented by a deep study of the chemical,

21 biochemical and microstructural transformations of the muscle and the effect that these

22 changes have on the electrical dispersions in radiofrequency range, may become

23 feasible for online DPM detection. For this paper, non-damaged and affected by DPM

chicken breasts (pectoralis major and pectoralis minor) was analysed. Permittivity in radiofrequency and microwave ranges were measured in the different tissues: pectoralis minor, major and skin in order to characterize them. Moreover, proteins content, ion content and pH were measured. With this data, a sensor for measuring the permittivity of chicken whole carcass with skin was developed; it consists of two pairs of two flat plates sensor connected to an impedance Agilent analyzer 4294A and can measure the permittivity from 40 Hz to 1 MHz. The results demonstrated the feasibility of the permittivity in radiofrequency range as an potential identification technique of chicken breasts affected by DPM.

Keywords: Deep Pectoral Myopathy, poultry, chicken meat, spectrophotometry, radiofrequency.

1. INTRODUCTION

The trend in meat consumption has changed drastically in the last years, mainly due to the relationship of red and processed meats with cancer and cardiovascular diseases (Rohrmann et al., 2013); this has caused a substantial growth in poultry meat sector and it is predicted that by 2024, the production will expand by 24% reaching of an additional of 26 Mt of poultry production (OECD/FAO, 2015). In order to face up this growing demand, poultry industry has accomplished genetic modifications, has increased the growth rate and has reduced the growing time by about 40 days or less (Petracci et al., 2015). Consequently, it has led to an increased in the appearance of muscular physiopathies such as white striping (Traffano-Schiffo et al., 2017), woody breast (Kuttappan et al., 2016) or Deep Pectoral Myopathy (Radaelli et al., 2016; Petracci et al., 2015).

49 Deep Pectoral Myopathy (DPM) is an ischemic hemorrhage or necrosis due to

50 inadequate blood supply of variously sized deep pectoral muscle (*pectoralis minor*).

51 The most common cause is a heart attack or an angina pectoris due to the stress and the

52 hypertrophy. The troubles with the muscle hypertrophy depends on the animal lineage

53 (Bianchi et al., 2006), however, the problematic stress level can be produced in the

54 poultry farm, due to the broiler activity, lighting, flapping, etc. (Petracci et al., 2017), or

55 during the transport of the birds to the slaughterhouse (driving of the truck, temperature

56 in boxes, etc.) (Cavani et al., 2009). If angina pectoris or infarct kills the bird the animal

57 does not reach the slaughterhouse, but if the infarct does not kill the animal the broiler is

58 processed, many times as a whole carcass, being rejected in the market and producing

59 several costs for the companies (Kijowski et al., 2014). Incidences in the industry are in

60 normal lineage 0.6% and in hypertrophy lineage 7% (Bailey et al., 2015), and

61 depending on the severity of DPM can be from lightly (20%) to severe (1%) (Bianchi et

62 al., 2006).

63 In this sense, a detection after the cooling tunnel (about 5 hour pmt), before classifying

64 the carcass for cutting or packaging as a whole carcass, would eliminate the losses of

65 carcasses sold with DPM, sending them to the cutting operation in order to approve the

66 undamaged meat of these animals that have suffered DPM (Fito et al., 2016). For this

67 purpose, it is necessary to classify the level of DPM damage. Therefore, according to

68 the nature of damage, muscles with DPM can be divided in two categories: 1.

69 haemorrhagic with haematomas and blood clots and 2. necrotic tissue (Kijowski et al.

70 2014).

71 Some researches were carried out with the objective to determine the DPM with non-

72 destructive technology. Firstly, Jones (1977) proposed a system based in an image

73 analyses by a probe (VIS range), obtaining an inaccurate image when the poultry

74   carcass has necrotic myopathies. However, the production rate of poultry industry has

75   made to this technology unable to be applicable to production lines (Kijowski et al.,

76   2014; Pastuszczak-Frak, & Uradzinski, 2009). Swatland and Lutte, (1984) have

77   proposed an equipment based on spectrophotometry using a fiber optic light guide to

78   measure the absorbance from 400 to 700 nm pushing the light guide into the muscle

79   samples and thus, damaging the minimum to the carcass; however the obtained results

80   were not satisfactory.

81   Currently, poultry industry still demands a fast and reliable equipment able to

82   discriminate and identify the poultry breasts affected with DPM in production lines. In

83   this sense, spectrophotometry in radiofrequency and microwave range could be a viable

84   option to face up this challenge. This technique allows obtaining the physical property

85   that describes the electric interactions of a photon flux with any biological system,

86   called permittivity. Permittivity is a vector property and can be expressed as a complex

87   number with the dielectric constant (ε') as the real term and the dielectric loss factor

88   (ε'') as the imaginary term. The dielectric constant is related to the ability of the

89   biological system to absorb and store electric energy, and the loss factor is related to the

90   dissipation of the electric energy in other energies, as thermal or mechanical (Talens et

91   al., 2016).

92   At frequencies between Hz and MHz (radiofrequency range), two main dispersions can

93   be identify, called α and β. In a simplified way, α-dispersion (from a few Hz to a few

94   kHz) represents the orientation of the mobile charges within the biological system

95   (Kuang, & Nelson, 1998) as electrolytes, acids or small molecules with charge. β-

96   dispersion (from kHz to MHz) describes the interactions of photon flux with the fixed

97   charges or low mobility charges that are found in the biological system; this dispersion

98   can be divided in two sections. In the kHz range, this dispersion includes the

99 interactions with the charges of structural macromolecules that make up the solid phase

100 of the system, such as proteins (Wolf et al., 2012). In the MHz range, the interactions of

101 charges associated to the surface tension of the solid surface in contact with the fluid

102 medium, called Maxwell-Wagner phenomenon (Traffano-Schiffo et al., 2018). This

103 technique has been already used to determine meat quality (Zhao et al., 2017; Damez, &

104 Clerjon, 2013; Samuel et al., 2012; Castro-Giráldez et al., 2010), meat ageing (Trabelsi

105 et al., 2014; Castro-Giráldez et al., 2011; Zhuang et al., 2007), and to monitor meat

106 drying process (Muradov et al., 2016; Muradov et al., 2015; Traffano-Schiffo et al.,

107 2015). Moreover, the applicability of this technique to identify white striping

108 physiopathy in chicken carcass has been demonstrated (Traffano-Schiffo et al., 2017).

109 The aim of this research was to develop a sensor for measuring the permittivity of

110 chicken whole carcass with skin in depth (crossing different tissues) and to determine its

111 feasibility to predict DPM myopathy in chicken carcasses.

112

113 **2. MATERIALS AND METHODS**

114 **2.1. Raw material**

115 Experiments were carried out using chicken carcasses provided by the slaughterhouse

116 Grupo Sada (Nutreco S.A.) located in Rafelbunyol, Valencia (Spain). After slaughter,

117 male broilers (from different flock of birds) of 42 d were bled, plucked and tempered in

118 a cooling tunnel at 4 ºC during 3 h. Later, chicken carcasses were transported to the

119 laboratory of the Institute of Food Engineering for Development (IuIAD) at the

120 Polytechnic University of Valencia (UPV) using isothermal bags with ice in order to

121 maintain the samples at 2 ± 2 ºC.

122

123 **2.2 Experimental Procedure**

124 The experimental procedure was divided into two stages; in the first stage, the carcasses

125 were dismembered and *Pectoralis minor* and *major* of the same animal were used to

126 carry out the experiment. An industrial trained expert classified the samples by the

127 visual appearance in damaged samples (samples with hemorrhages, blood clots, and

128 necrosis) and non-damaged (normal) samples (category 0). Within the damaged

129 samples, samples were classified in necrotic samples or category 2 (samples with any

130 necrotic area) and hemorrhagic samples with hematomas and blood clots or category 1

131 (in this category, the remaining damaged samples that were not classified in the

132 category 2 were included). 70 chickens were analyzed: 30 correspond to non-damaged

133 tissues, 20 to category 1 and 20 to category 2. The permittivity of the samples was

134 measured at 16 h of post-mortem time (pmt) in *Pectoralis minor* and *major* of the same

135 animal in order to characterize electrically the different chicken tissues. Permittivity was

136 measured in radiofrequency and microwaves ranges at 4 ºC. In radiofrequency range

137 (from 40 Hz to 1 MHz), a sensor with two needles with blunt-ended was used

138 (Traffano-Schiffo et al., 2017). In microwave range (from 500 MHz to 20 GHz), an

139 Agilent 85070E open-ended coaxial probe was used to measure the permittivity.

140 Microstructural analyses of damaged and non-damaged tissue from damaged and non-

141 damaged samples with 16 h of pmt were carried out in *Pectoralis minor*. At 16 h of pmt,

142 the pH, moisture, protein and ion content were measured in *Pectoralis minor* and *major*

143 (from three different positions of the Pectoralis in order to obtain a representative

144 value).

145 In the second stage, 105 carcasses (35 per category) were used for the experiments. In

146 the cutting room of the slaughterhouse, the chicken carcasses were opened by the

147 central front area, and a trained expert inspected visually the pectoralis muscles,

148 separating those carcasses whose pectoralis minor belonged to categories 0, 1 and 2.

149 After visual inspection and once the samples were classified, the carcasses were

150 assembled recovering its original shape to the maximum for its later measurement in the

151 laboratory. Each carcass was formed by its bone structure, Pectoralis minor, major and

152 its skin. All the carcasses were kept at 4 ℃ until its analysis in the laboratory.

153 Permittivity of the carcasses with skin was measured from 8 to 18 h of pmt, taking

154 measurements every two hours, with a curved sensor designed and constructed for this

155 purpose (see Results Section). Samples were maintained at 4 ± 1 ℃ during the

156 experimental procedure.

157

158 **2.3. Physical Measurements**

159 Moisture was accomplished following the ISO 1442 (1997), i.e. drying the samples at

160 110 ℃ at atmospheric pressure during 48 hours until a constant weight was reached.

161 The pH of samples was measured with a punch pH-metre S-20 SevenEasy™ (Mettler

162 Toledo, Barcelona, Spain). It is possible to relate lactate content with pH values for

163 poultry breast meat from 1 to 24 hours of pmt (Huang et al., 2014). Therefore,

164 lactate content for each sample was obtained using the following equation:

165
$$x_{lactate} = -29.566\,pH + 233.98 \tag{1}$$

166 Being $x_{lactate}$ the lactate content expressed in μmol/g.

167 All determinations were made in triplicate.

168 It is important to take into account that not only the lactate metabolism affects to the

169 pH; also the ATP depletion metabolism, producing phosphates reduces the pH.

170 **2.4. Differential Scanning Calorimetry (DSC)**

171 Proteins phase transitions were calculated using a differential scanning calorimeter

172 Mettler Toledo DSC 1 (Mettler Toledo, Barcelona, Spain) provided with the full range

173 temperature sensor FRS5. The calibration of the equipment was performed by the

174   automatic calibration function FlexCal supplied by the manufacturers. Samples of

175   around 20-30 mg were enclosed in hermetically sealed aluminium pans (Mettler Toledo,

176   ME-00026763) and then loaded onto the equipment at room temperature. An empty

177   hermetically sealed pan was used as the reference sample and also to run the blank

178   curve.

179   In the experiments, samples were heated from 15 to 115 °C at a heating rate of 10

180   °C/min under N_2 (flowed at 200 min/mL) in order to evaluate the protein state within

181   meat muscle. All determinations were performed in triplicate.

182   Once the scans were finished, analyses of the samples were carried out by the STARe

183   software fitted with the DSC equipment. The following initial denaturalization

184   temperatures were considered: myosin 55 ºC, collagen and sarcoplasmic proteins

185   between 63 to 76 ºC and actin 79-80 ºC (Ross, 2006; Fernández-Martín et al., 2000).

186   Mass fraction of proteins: myosin, collagen and sarcoplasmic, and actin from Pectoralis

187   minor and major were obtained from the transition energies obtained by DSC and the

188   latent heat of denaturation of the pure proteins (Ross, 2006; Fernández-Martín et al.,

189   2000) according to Equation (2):

190    $$x_{protein} = \frac{E}{\Delta G°denat} \tag{2}$$

191   Being $x_{protein}$ the mass fraction of each protein: myosin, collagen and sarcoplasmic

192   ($kg_{protein}/kg_{total}$), and actin; E the transition energy of specific protein (J/g_{total}) obtained

193   from the thermogram; and the $\Delta G^{o,denat}$ the latent heat of denaturation of each pure

194   structured protein ($J/g_{protein}$), being: 13.9, 16.5, and 14.5 for myosin, collagen and

195   sarcoplasmic, and actin, respectively .

196

197   **2.5. Analyses of microstructural changes: Low-temperature scanning electron**

198   **microscopy (Cryo-SEM).**

199   Microstructure of non-damaged and DPM samples were analyzed by Cryo-SEM. A

200   Cryostage CT-1500C unit (Oxford Instruments, Witney, UK), coupled to a Jeol JSM-

201   5410 scanning electron microscope (Jeol, Tokyo, Japan), was used. The sample was

202   immersed in slush N_2 (-210 ℃) and then quickly transferred to the Cryostage at 1 kPa

203   where sample fracture took place. The sublimation (etching) was carried out at -95 ℃.

204   The final point was determined by direct observation in the microscope, working at 5

205   kV. Then, once again in the Cryostage unit, the sample was coated with gold in vacuum

206   (0.2 kPa), applied for 3 min, with an ionization current of 2 mA. The observation in the

207   scanning electron microscope was carried out at 20 kV, at a working distance of 15 mm

208   and a temperature ≤ -130 ℃.

209

210   **2.6. Ion content by ion exchange chromatography**

211   Ion quantification was carried out by means of an ion IC chromatograph (Methrom,

212   Herisau, Switzerland), equipped with electronic detectors. For the determination of Li^+,

213   Na^+, Ca^{2+}, NH_4^+, K^+ and Mg^{2+} a universal standard Metrosep C2-150 (4.0 × 150 mm)

214   column (Methrom, Herisau, Switzerland) was used and for lactate content was used a

215   column Shodex$^®$ IC SI-50 4E (4,0 × 250 mm, Tokio, Japan). The eluent used was

216   composed of tartaric acid (4.0 mmol/L) and dipicolinic acid (0.75 mmol/L). In every

217   case, the chicken meat samples were previously homogenized at 9000 rpm in an

218   ULTRATURRAX T25 for 10 min and centrifuged (J.P. Selecta S.A., Medifriger-BL,

219   Barcelona, Spain) at 10000 rpm for 20 min. Afterwards, 1 mL of supernatant was

220   diluted with Milli$^®$-Q water in a 50 mL volumetric flask. The clarified extract was

221   filtered through a 0.45 μm Millipore filter. Finally, 15 mL was used to analyse the

222   cation content. The software ICnet 2.0 was used to analyse the results. High-purity Li^+,

223   Na^+, Ca^{2+}, NH_4^+, K^+, Mg^{2+} (Reagecon, Clare, Ireland) and lactate (Sigma-Aldrich Co.,

224   Madrid, Spain) standards were used to obtain the calibration curves.

225   Measurements were taken in triplicate.

226

227   **2.7. Permittivity measurements**

228   For the first stage, the permittivity was measured in radiofrequency range with a sensor

229   that consist on two needles with blunt-ended (Traffano-Schiffo et al., 2017). The sensor

230   was connected to a 4694A impedance analyzer (Agilent, Santa Clara, CA, USA). The

231   frequency range measured was from 40 Hz to 1 MHz. Calibration of the equipment was

232   performed in open (air) and short-circuit.

233   The vectorial variable obtained by the Agilent analyzer is the impedance Z. The

234   impedance as a complex number is $\bar{Z} = R + jX$, where the real part of the impedance

235   is the resistance R and the imaginary part is the reactance X. Vectorial permittivity was

236   estimated from the vectorial impedance measurements using Equations (3), (4) and (5),

237   where variables R and X were transformed in ε', ε'' as follows:

$$\varepsilon' = \frac{-X}{(R^2 + X^2)} \frac{1}{2\pi C_0} \tag{3}$$

$$\varepsilon'' = \frac{R}{R^2 + X^2} \frac{1}{2\pi f C_0} \tag{4}$$

$$C_0 = \frac{\varepsilon_0 \, S}{d} \tag{5}$$

238   where f is the frequency (Hz), C_0 is the capacitance in the vacuum (F), S is the surface

239   of the electrodes (m^2), ε_0 is the vacuum permittivity (F/m) and d is the separation

240   between the electrodes with differential tension ($V_H - V_L$) (m).

241   For Microwave range, permittivity was measured from 500 MHz to 20 GHz with an

242   Agilent 85070E open-ended coaxial probe (Agilent, Santa Clara, CA, USA) connected

243   to an Agilent E8362B Vector Network Analyzer (Agilent, Santa Clara, CA, USA). The

244   system was calibrated using three different types of loads: open (air), short-circuit and 4

245   ºC Milli®-Q water. Once the calibration was carried out, 4 ºC Milli®-Q water was

246   measured again to check calibration suitability.

247   Permittivity measurements were performed in triplicate.

248

249   **2.8. Dielectric constant modeling**

250   The dielectric constant spectra were modelled adjusting the experimental data with the

251   model of Traffano-Schiffo et al. (2017):

$$l\varepsilon'(\omega) = l\varepsilon'_\infty + \sum_{n=1}^{3} \frac{\Delta l\varepsilon'_n}{1 + e^{((l\omega^2 - l\omega_\tau^2)*\alpha_n)}} \tag{6}$$

252   where $l\varepsilon'$ represents the decimal logarithm of the dielectric constant, $l\varepsilon'_\infty$ the logarithm

253   of the dielectric constant at high frequencies, $l\omega$ represents the decimal logarithm of the

254   angular velocity (obtained from the frequency), $\Delta l\varepsilon'_n$ ($\Delta l\varepsilon'_n = \log \varepsilon'_n - \log \varepsilon'_{n-1}$) the

255   magnitude of the dispersion, $l\omega_t$ the logarithm of the angular velocity at relaxation time

256   for each dispersion n, and α_n are the dispersion slopes.

257   With the parameters obtained from the model, it was possible to determine the

258   relaxation frequencies and dielectric constants of each relaxation (Equations (7) to

259   (10)):

$$\varepsilon'_\alpha = 10^{\left(l\varepsilon'_\infty + \Delta l\varepsilon'_\gamma + \Delta l\varepsilon'_\beta + \frac{\Delta l\varepsilon'_\alpha}{2} \right)} \tag{7}$$

$$\varepsilon'_\beta = 10^{\left(l\varepsilon'_\infty + \Delta l\varepsilon'_\gamma + \frac{\Delta l\varepsilon'_\beta}{2} \right)} \tag{8}$$

$$\varepsilon'_\gamma = 10^{\left(l\varepsilon'_\infty + \frac{\Delta l\varepsilon'_\gamma}{2} \right)} \tag{9}$$

$$f_i = 10^{\frac{l\varpi_{\tau i}}{2 \cdot \pi}} \tag{10}$$

260   Being i for Equation (10) each dispersion (α, β and γ).

261

262 **2.8. Statistical analysis**

263 The statistical analysis was carried out with the Statgraphics Centurion XVI Software

264 (Statgraphics, Virgina, U.S.A.). One-Way ANOVA analyses were made in order to find

265 statistically significant differences between the studied parameters. The logistic

266 Traffano-Schiffo model (Traffano-Schiffo et al., 2017) was fitted by using nonlinear

267 regression.

268 **2.9 Penetration depth analysis.**

269 The COMSOL Multiphysics finite element-based electromagnetics were used in order

270 to obtain the penetration depth.

271

272 **3. RESULTS**

273 Depending on the time without blood flow after an ischemic episode, the muscle tissue

274 can recover its whole structural activity (less than 15 min) or a permanent damage can

275 be produced. If the damage is low, blood clots, hematoma or hemorrhagic tissue appear

276 (red tissue), if the damage is high, the rupture of the tissue with necrotic process in

277 muscle (green tissue) is produced (Bilgili and Hess, 2008). In order to detect the

278 ischemic processes produced in muscle tissue, by radiofrequency spectrophotometry, it

279 is necessary to follow the chemical species involved in this biological process that also

280 interact with photons in this frequency range. Figure 1 shows the muscle fibers

281 packaged by collagen for the three categories studied at 16 h pmt.

282

283 Figure 1b shows on the left a slight degradation of the fibers and on the right shows an

284 accumulation of blood clots (pointed with rows) with the consequent degradation of the

285 sarcoplasmic proteins (as shows table 1). In the case of the necrotic muscle, Figure 1c

286 (pointed with rows and circle), severe degradation of fibers and collagen is observed,

287   breaking the cell packing of fibers. Therefore, it will be important to follow the

288   degradation of proteins because, due to their chemical nature, they interact with photons

289   in the β-dispersion frequency range.

290

291   The protein mass fraction per each group of samples was estimated by DSC. However,

292   this technique does not allow to discriminate between collagen and sarcoplasmic

293   proteins and both groups are different and have different activities in the meat

294   transformations. Ageing process and myopathies produce degradation in the structural

295   proteins, and it is possible to determine the effect of the myopathy comparing the

296   protein state of damaged tissue with normal tissue at the same pmt. Table 1 shows the

297   mass fraction of each structural protein (myosin, actin, collagen and sarcoplasmic

298   proteins) in normal tissue, hemorrhagic with hematomas and/or blood clots samples and

299   necrotic samples, where it is possible to observe how the quantity of myosin decreases

300   in *Pectoralis minor* depending on the level of damage. While, necrotic samples show a

301   higher decrease of the collagen and sarcoplasmic proteins contents comparing with

302   normal tissue in *Pectoralis minor*. This result can be related with the high level of

303   degradation in the collagen observed in the micrographies showed in Figure 1c. Similar

304   results were obtained in the research developed in 1990 by Takahashi et al (1990). With

305   regard to *Pectoralis major*, a significant decrease in myosin content is appreciated in

306   necrotic tissue comparing with the others two categories. Collagen and sarcoplasmic

307   proteins also show a significant decrease comparing to hemorrhagic samples. Finally,

308   actin degradation of damaged categories is significant higher with regard to the normal

309   samples both in *Pectoralis minor* and in *major*.

310   In order to explain the α-dispersion, it is necessary to quantify all the chemical species

311   with high ionic strength and enough relative mass. Table 2 shows the most important

312 chemical species with the capacity to produce α-dispersion. During the process of meat

313 maturation, associated with the lack of blood supply, the pH decreases related with the

314 anaerobic lactate production and the consumption of ATP with the consequent

315 production of phosphate ions (Smulders et al., 2014). It has not been possible to

316 quantify the production of phosphate ions, however, the pH value measured is the

317 addition of the lactate and the phosphate ion and the production of both is related with

318 the anaerobic respiration pathway and therefore both chemical species are an indicator

319 in Pectoralis major and minor of the level of maturation that has occurred in each tissue.

320

321 The tissue that has suffer an ischemic process presents an increase in the electrolytes

322 content associated with the biological activity of the fibers, from the transport channels

323 (Horimoto et al., 2000; Gürke et al., 2000; Immke, & McCleskey, 2001) as well as the

324 signaling processes (Berchtold et al., 2000). This is due to the partial or total rupture of

325 cell packing and some organelles such as mitochondria (Miyoshi et al., 1992) increasing

326 the concentration of free ions. However, these variations are smaller compared to the

327 associated with the lactate that governs the ionic force of the medium.

328 Spectrophotometric measurements of the different tissues have been made in the

329 complete radiofrequency and microwave spectrum (Figure 2) where it is possible to

330 observe the difference between each tissue. The algorithm of Traffano-Schiffo et al.

331 (2017) has been applied in order to obtain the relaxations of the dispersions α, β and γ.

332 The chemical specie with the higher capacity to change the ionic strength of the medium

333 is lactate (see Table 2), for this reason it is possible to quantify the production of lactate

334 (it means, the cellular anaerobic metabolism of fibers) through the variation of the

335 dielectric constant in relaxation of the α-dispersion.

336

337   In Figure 3, it is possible to observe a direct relationship between the electrical constant

338   and the lactic content produced in cellular anaerobiosis. The necrotic tissue, without

339   organic capacity to metabolize glycogen and therefore produce lactate, remain a low

340   ionic strength in the liquid cell medium, reducing the capacity to store electrical energy.

341   In case of hemorrhagic samples, the anaerobic metabolism is lower than the normal

342   tissue (see Table 2) but it still has a high production of lactate; finally, the normal tissue

343   shows normal production of lactate associated with its pmt. For this reason, it is

344   possible to use measures in α-dispersion to recreate the anaerobic metabolism, and to

345   predict the state of fiber cells.

346   In the case of β-dispersion, it is possible to follow the conformational changes of the

347   charged macromolecules, in meat case corresponds to protein. Figure 4 shows the

348   collagen and sarcoplasmic proteins content together (Figure 4a) and myosin protein

349   content (Figure 4b) versus the dielectric constant in relaxation of the β-dispersion. The

350   higher the level of denaturation of any of these proteins, the lower the capacity of the

351   system to store electrical energy since these proteins lose charges when they are

352   denatured (Traffano-Schiffo et al., 2017). It is possible to appreciate how the ischemic

353   categories (DPM) have significantly lower values of dielectric constant than normal

354   samples, being able to differentiate clearly.

355

356   The γ-dispersion describes electrical interactions of photons with dipolar molecules, in

357   the case of biological tissues this molecule is water, therefore any variation in the

358   content or mobility of water can be quantified analyzing the vectorial permittivity in this

359   dispersion. The ischemic processes do not show great changes in the water retention or

360   adsorption, but the broken tissues will have less surface to be able to adsorb water and

361   therefore lower moisture values. Figure 5 shows the relation between the dielectric

362   constant in the relaxation of γ-dispersion with the moisture for the three sample

363   categories, where it is possible to observe a linear relationship between them. In this

364   figure the category of hemorrhagic muscle or angina shows lower moisture and lower

365   value of dielectric constant, intermediate values the category of necrotic muscle or

366   infarction and finally the highest value of moisture and dielectric constant corresponds

367   to normal samples. This correlation can be due to the level of integrity of each tissue

368   (necrotic tissue more unstructured and normal tissue fully conformed), affecting to the

369   water retention capacity of each tissue.

370

371   Once the behavior of each tissue and each biological metabolism associated with muscle

372   maturation and ischemic processes has been described, it has been necessary to develop

373   a device capable of measuring the spectrophotometric properties in radiofrequency

374   range, in depth, in order to quantify infarct damage or chest angina in the pectoralis

375   minor measured in whole chicken carcasses.

376   For this purpose, a device was developed and patented by the authors,

377   WO2017125633A1 (Fito et al., 2016). It consists on a non-destructive sensor of two

378   pairs of flat plates electrodes, each pair has different size and distance between them in

379   order to obtain different penetration depth and therefore, the device is capable of

380   measuring the different muscle tissues. It has a curved design made it by a 3D printer,

381   so it perfectly fits to the curvature of the poultry pectoral muscles. The sensor was

382   connected to an impedance analyzer Agilent 4294A (Figure 6) and the frequency range

383   measured was from 40 Hz to 1 MHz. Calibration of the equipment was performed in

384   open (air) and short-circuit. The measurements require contact on the carcass, being

385   able to make the measurements online by any multiple classifier to allow the sensor to

386   contact to the carcass because the measurement time is very fast, less than 10 ms.

387

As Figure 6a shows, the device performs measurements in two sensor configurations (IN-OUT), changing the penetration depth. Position IN refers to the smallest electrodes, which have lower distance between them, able to measure only the Pectoralis major. In contrast, position OUT refers to the biggest electrodes with higher distance between them, able to measure Pectoralis minor. The operation of the circuit is described in Figure 6b and the penetration depth is shown in Figure 6c. More technical aspects are described in Fito et al., 2016. The penetration depth was estimated by Maxwell algorithms using the permittivity previously obtained from each tissue (Figure 2). Spectrophotometric measurements of the breast carcasses have been made in the radiofrequency range (Figure 7) by using the new device with the IN configuration to obtain the dielectric properties of the *pectoralis major* (Figure 7a) and with the OUT configuration to obtain a mix of dielectric properties of *pectoralis major* and *minor* (Figure 7b). Comparing both measures it is possible to obtain the dielectric properties of *pectoralis minor*. The algorithm of Traffano-Schiffo et al. (2017) has been applied in order to obtain the relaxations of the α and β dispersions.

With the measurements obtained from the device in IN and OUT configuration, and with post mortem time, a predictive multi-factorial algorithm was developed (Fito et al., 2016). The predictive result of the algorithm is shown in Figure 8. As seen in Figure 8, When comparing the real categories of the samples at different postmortem times and those predicted with the spectrophotometric measurements, the correct segregation by predictive categories of the samples is shown.

4. CONCLUSIONS

412 It has been related the main metabolisms of muscle/meat transformation affected by the

413 DPM disease (anaerobic metabolism, ATP depletion metabolism and structural proteins

414 transformations) with the vectorial permittivity in radiofrequency range. First

415 metabolisms produce two low molecular weight chemical species with a high ionic

416 strength and mobility (lactate and phosphates), where their high interaction with

417 photons in alpha dispersion has been demonstrated. Moreover, the structural proteins,

418 molecules of high molecular weight strongly charged with high orientation capacity and

419 no mobility have been related with the properties of photons in beta dispersion.

420 A multi-sensor device for measuring the dielectric properties in depth of whole chicken

421 carcass with skin was developed; it consists of two pairs of two flat plates sensor

422 connected to an impedance Agilent analyzer 4294A and can measure the vectorial

423 permittivity from 40 Hz to 1 MHz. The results demonstrated the feasibility of the

424 vectorial permittivity in radiofrequency range as an identification technique of chicken

425 breasts affected by DPM, in whole carcass with skin, obtaining the measures in depth,

426 crossing different kinds of tissues.

427

437

6. REFERENCES

Berchtold, M. W., Brinkmeier, H., & Müntener, M. (2000). Calcium ion in skeletal muscle: its crucial role for muscle function, plasticity, and disease. *Physiological Reviews*, 80(3), 1215-1265.

Bianchi, M., Petracci, M., Franchini, A., & Cavani, C. (2006). The occurrence of deep pectoral myopathy in roaster chickens. *Poultry Science*, 85(10), 1843-1846.

Bilgili, S. F., & Hess, J. (2008). Green muscle disease. Reducing the incidence in broiler flock. Ross Tech, 8(48), 3.

Castro-Giráldez, M., Botella, P., Toldrá, F., & Fito, P. (2010a). Low-frequency dielectric spectrum to determine pork meat quality. *Innovative Food Science & Emerging Technologies*, 11(2), 376-386.

Castro-Giráldez, M., Toldrá, F., & Fito, P. (2011). Low frequency dielectric measurements to assess post-mortem ageing of pork meat. *LWT-Food Science and Technology*, 44(6), 1465-1472.

Cavani, C., Petracci, M., Trocino, A., & Xiccato, G. (2009). Advances in research on poultry and rabbit meat quality. *Italian Journal of Animal Science*, *8*, 741-750.

Damez, J. L., & Clerjon, S. (2013). Quantifying and predicting meat and meat products quality attributes using electromagnetic waves: An overview. *Meat Science*, 95(4), 879-896.

Fernández-Martín, F., Fernández, P., Carballo, J., & Jiménez-Colmenero, F. (2000). DSC study on the influence of meat source, salt and fat levels, and processing parameters on batters pressurisation. *European Food Research and Technology*, 211(6), 387-392.

Fito, P.J., Colom, R.J., Castro-Giraldez, M., Herrero, V., Monzó, J.M., Traffano-Schiffo, M.V., Tébar, A., (2016). Device and method for detecting damage caused by deep pectoral myopathy in birds. World Patent, WO2017125633A1.

Gabriel, S.; Lau, R. W.; Gabriel, C. (1996). The dielectric properties of biological tissues: III. Parametric models for the dielectric spectrum of tissues. *Physics in Medicine and Biology*. 41(11), 2271.

Gürke, L., Mattei, A., Chaloupka, K., Marx, A., Sutter, P. M., Stierli, P., ... & Heberer, M. (2000). Mechanisms of ischemic preconditioning in skeletal muscle. *Journal of Surgical Research*, 94(1), 18-27.

Horimoto, H., Gaudette, G. R., Saltman, A. E., & Krukenkamp, I. B. (2000). The role of nitric oxide, K+ ATP channels, and cGMP in the preconditioning response of the rabbit. *Journal of Surgical Research*, 92(1), 56-63.

Huang, J. C., Huang, M., Wang, P., Zhao, L., Xu, X. L., Zhou, G. H., & Sun, J. X. (2014). Effects of physical restraint and electrical stunning on plasma corticosterone, postmortem metabolism, and quality of broiler breast muscle. *Journal of Animal Science*, 92(12), 5749-5756.

Immke, D. C., & McCleskey, E. W. (2001). Lactate enhances the acid-sensing Na+ channel on ischemia-sensing neurons. *Nature Neuroscience*, 4(9), 869-870.

ISO 1442:1997. (1997). Methods of test for meat and meat products. Determination of moisture content. BS 4401-3:1997.

JONES J.M. (1977). Quick detection now for 'Oregon disease'. *Poultry Industry* (pp. 14-15).

Kijowski, J., Kupińska, E., Stangierski, J., Tomaszewska-Gras, J., & Szablewski, T. (2014). Paradigm of deep pectoral myopathy in broiler chickens. *World's Poultry Science Journal*, 70(01), 125-138.

486   Kuang, W., & Nelson, S. O. (1998). Low-frequency dielectric properties of biological

487   tissues: a review with some new insights. *Transactions of the ASAE-American Society*

488   *of Agricultural Engineers*, 41(1), 173-184.

489   Kuttappan, V. A., Hargis, B. M., & Owens, C. M. (2016). White striping and woody

490   breast myopathies in the modern poultry industry: a review. *Poultry Science*, 95(11),

491   2724-2733.

492   Miyoshi, Y., Nakaya, Y., Wakatsuki, T., Nakaya, S., Fujino, K., Saito, K., & Inoue, I.

493   (1992). Endothelin blocks ATP-sensitive K+ channels and depolarizes smooth muscle

494   cells of porcine coronary artery. *Circulation Research*, 70(3), 612-616.

495   Muradov, M., Cullen, J. D., Shaw, A., Korostynska, O., Mason, A., Al-Shamma'a, A. I.,

496   & Alvseike, O. (2015). Online non-destructive monitoring of meat drying using

497   microwave spectroscopy. In 9th International Conference on Sensing Technology,

498   Auckland, NZ.

499   Muradov, M., Cullen, J., & Mason, A. (2016). Real-Time Monitoring of Meat Drying

500   Process Using Electromagnetic Wave Sensors. In S. C. Mukhopadhyay (Ed.), *Next*

501   *Generation Sensors and Systems* (pp. 221-233). Springer International Publishing,

502   Palmerston North.

503   OECD-FAO. 2015. OECD-FAO Agricultural Outlook 2015, OECD Publishing, Paris.

504   pp. 41. doi: 10.1787/agr outlook-2015-en.

505   Pastuszczak-Frak, M., & Uradzinski, J. (2009). Influence of green muscle disease on

506   quality of meat subjected to thermal treatment. *Polish Journal of Veterinary Sciences*,

507   12(4), 527-530.

508   Petracci, M., & Cavani, C. (2012). Muscle growth and poultry meat quality issues.

509   *Nutrients*, 4(1), 1-12.

510   Petracci, M., Mudalal, S., Soglia, F., & Cavani, C. (2015). Meat quality in fast-growing

511   broiler chickens. *World's Poultry Science Journal*, 71(02), 363-374.

512   Petracci, M., Soglia, F., & Berri, C. (2017). Muscle metabolism and meat quality

513   abnormalities. In M. Petracci, C. Berri (Eds.), *Poultry Quality Evaluation* (pp. 51-75).

514   Woodhead Publishing https://doi.org/10.1016/B978-0-08-100763-1.00017-9

515   Radaelli, G., Piccirillo, A., Birolo, M., Bertotto, D., Gratta, F., Ballarin, C., ... &

516   Trocino, A. (2016). Effect of age on the occurrence of muscle fiber degeneration

517   associated with myopathies in broiler chickens submitted to feed restriction. *Poultry*

518   *Science*, 1-11.

519   Rohrmann, S., Overvad, K., Bueno-de-Mesquita, H. B., Jakobsen, M. U., Egeberg, R.,

520   Tjønneland, A., ... & Palli, D. (2013). Meat consumption and mortality-results from the

521   European Prospective Investigation into Cancer and Nutrition. *BMC medicine*, 11(1), 1.

522   Ross, Y. H. (2006). Phase transitions and transformations in food systems. In D. R.

523   Heldman, D. B. Lund (Eds.), *Handbook of Food Engineering* (pp. 287-352). CRC

524   Press, FL.

525   Samuel, D., Trabelsi, S., Karnuah, A. B., Anthony, N. B., & Aggrey, S. E. (2012). The

526   use of dielectric spectroscopy as a tool for predicting meat quality in poultry.

527   *International Journal of Poultry Science*, 11(9), 551.

528   Smulders, F., Hofbauer, P. & Geesink, G. H. (2014). The Conversion of Muscle to

529   Meat. In T. Ninios, J. Lundén, H. Korkeala, & M. Fredriksson-Ahomaa (Eds.), *Meat*

530   *Inspection and Control in the Slaughterhouse* (pp. 399-421). Oxford.

531   Swatland, H. J., & Lutte, G. H. (1984). Optical characteristics of deep pectoral

532   myopathy in turkey carcasses. *Poultry Science*, 63(2), 289-293.

533   Takahashi, S., Barry, A. C., & Factor, S. M. (1990). Collagen degradation in ischaemic

534   rat hearts. *Biochemical Journal*, 265(1), 233-241.

535   Talens, C., Castro-Giraldez, M., & Fito, P. J. (2016). Study of the effect of microwave

536   power coupled with hot air drying on orange peel by dielectric spectroscopy. *LWT-Food*

537   *Science and Technology*, 66, 622-628.

538   Trabelsi, S., Roelvink, J., & Russell, R. B. (2014). Investigating the influence of aging

539   on radiofrequency dielectric properties of chicken meat. *Journal of Microwave Power*

540   *and Electromagnetic Energy*, 48(4), 215-220.

541   Traffano-Schiffo, M. V., Castro-Giraldez, M., Colom, R. J., & Fito, P. J. (2017).

542   Development of a Spectrophotometric System to Detect White Striping Physiopathy in

543   Whole Chicken Carcasses. *Sensors*, 17(5), 1024.

544   Traffano-Schiffo, M. V., Castro-Giraldez, M., Colom, R. J., & Fito, P. J. (2015). Study

545   of the application of dielectric spectroscopy to predict the water activity of meat during

546   drying process. *Journal of Food Engineering*, 166, 285-290.

547   Traffano-Schiffo, M. V., Castro-Giraldez, M., Colom, R. J., & Fito, P. J. (2018). New

548   Spectrophotometric System to Segregate Tissues in Mandarin Fruit. *Food and*

549   *Bioprocess Technology*, 11(2), 399-406.

550   Wolf, M., Gulich, R., Lunkenheimer, P., & Loidl, A. (2012). Relaxation dynamics of a

551   protein solution investigated by dielectric spectroscopy. *Biochimica et Biophysica Acta*

552   *(BBA)-Proteins and Proteomics*, 1824(5), 723-730.

553   Zhao, X., Zhuang, H., Yoon, S. C., Dong, Y., Wang, W., & Zhao, W. (2017). Electrical

554   Impedance Spectroscopy for Quality Assessment of Meat and Fish: A Review on Basic

555   Principles, Measurement Methods, and Recent Advances. *Journal of Food Quality*,

556   2017, 16. https://doi.org/10.1155/2017/6370739

557   Zhuang, H., Nelson, S. O., Trabelsi, S., & Savage, E. M. (2007). Dielectric properties of

558   uncooked chicken breast muscles from ten to one thousand eight hundred megahertz.

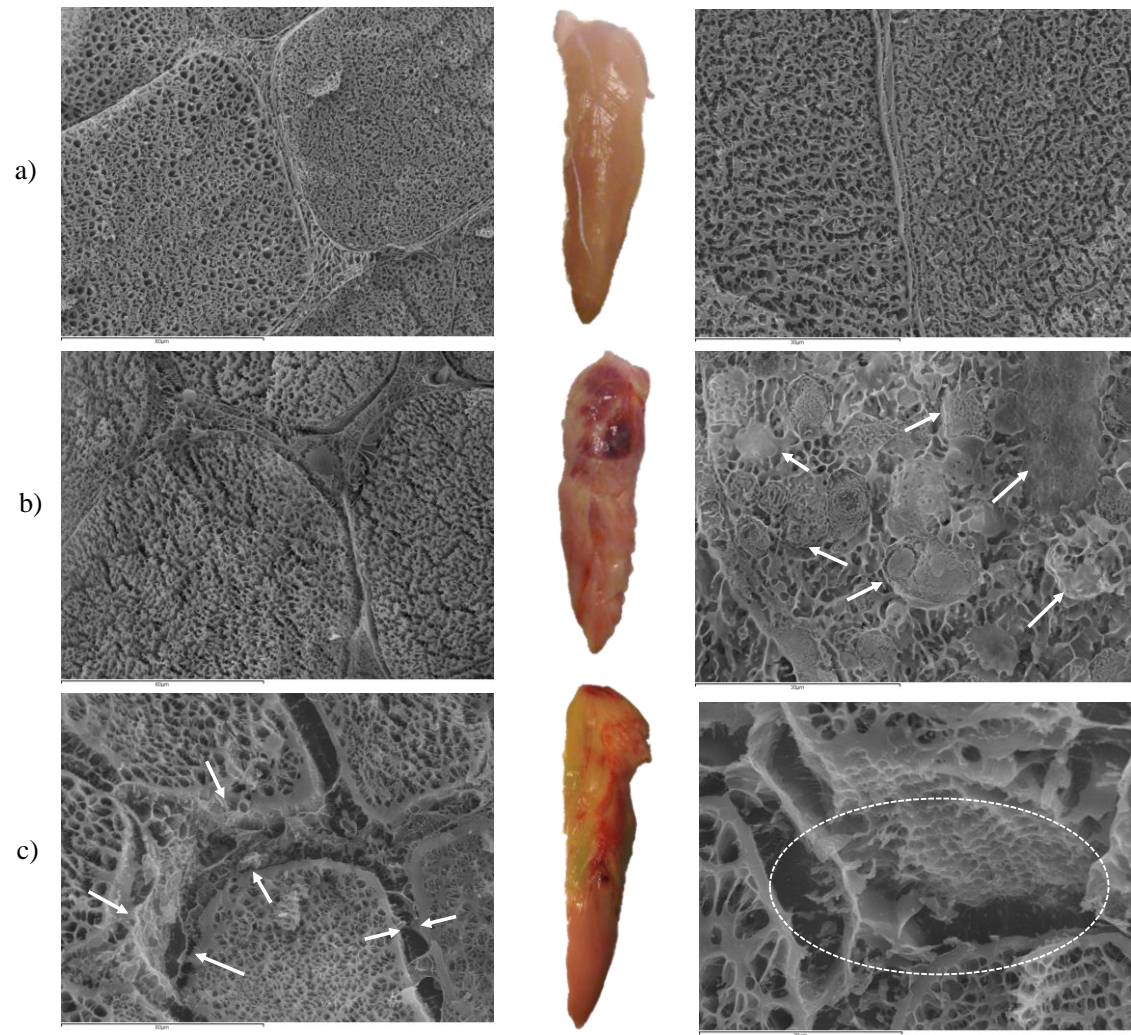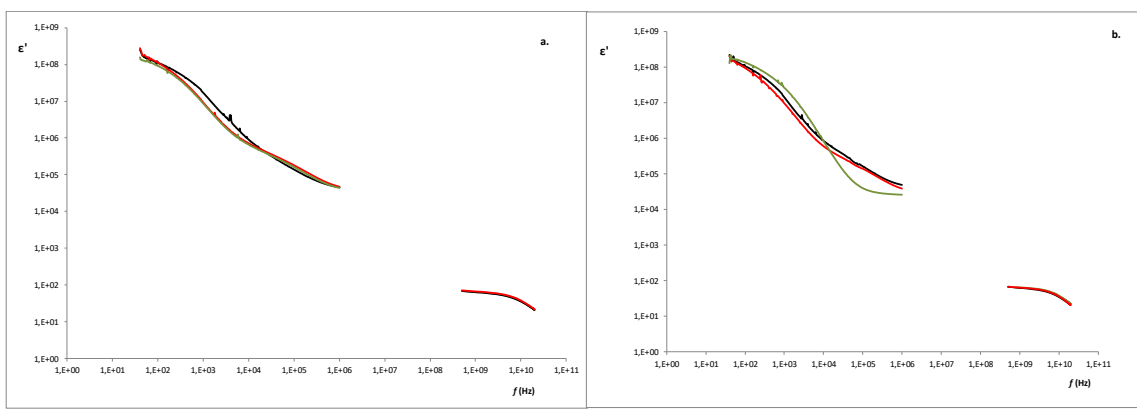559   *Poultry Science*, 86(11), 2433-2440.

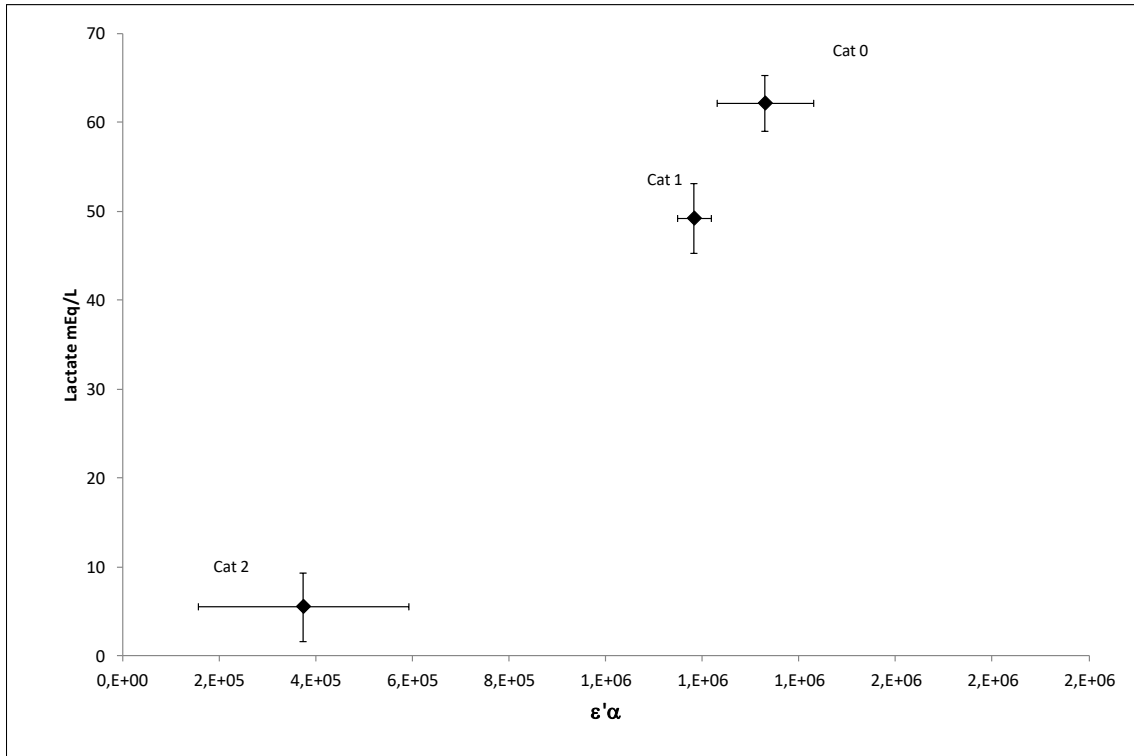**Figure 1**

Figure 1.

Figure 2

Figure 2

Figure 3

Figure 3.

Figure 4
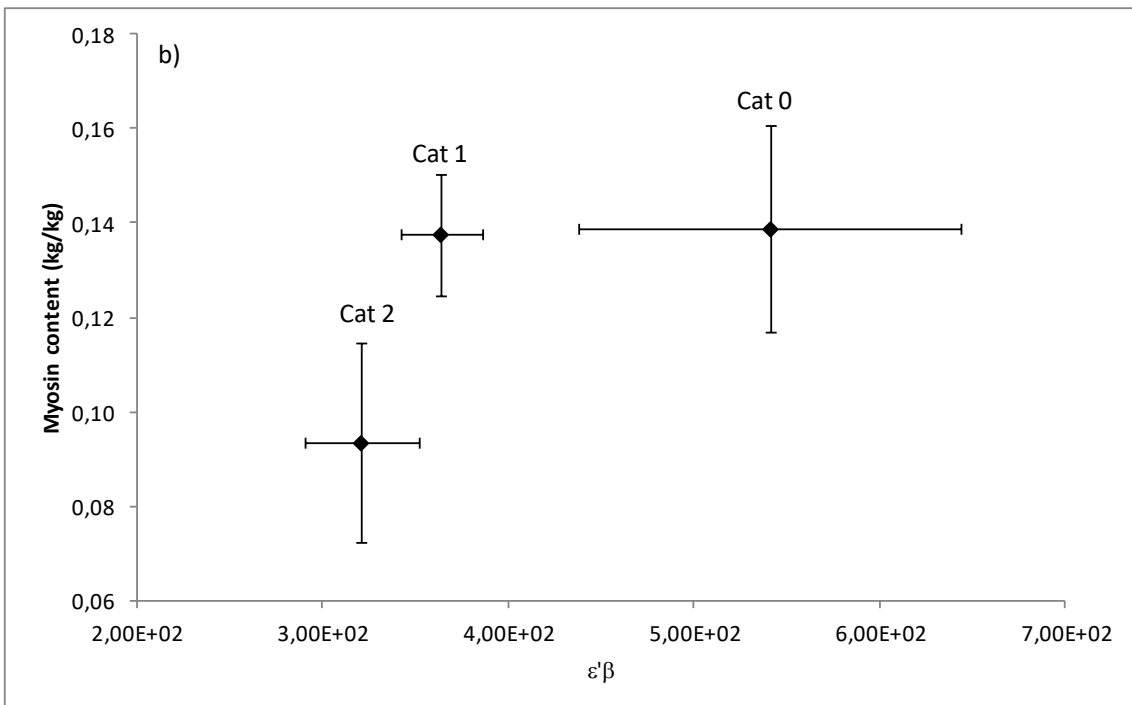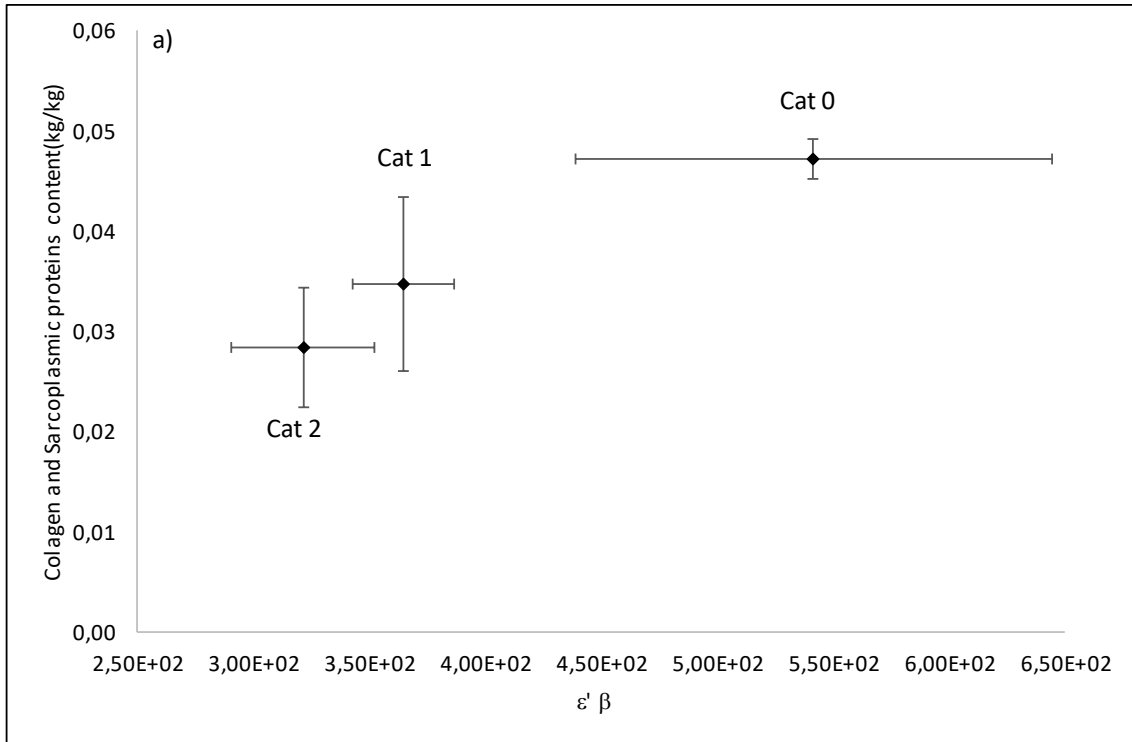
Figure 4

Figure 5

Figure 5

Figure 6

a.

OUT ◼ IN

Skin

Pectoralis major

Pectoralis minor

b. Electric circuit

I_L V_L V_H I_H

V

A

c.

Penetration Depth

Pectoralis major
Pectoralis minor

Pectoralis major
Pectoralis minor

d.
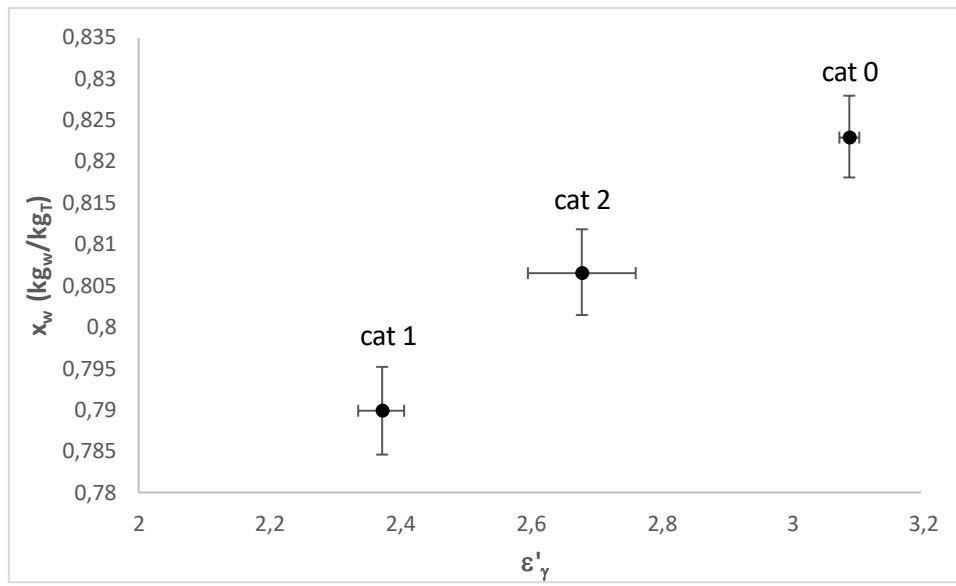
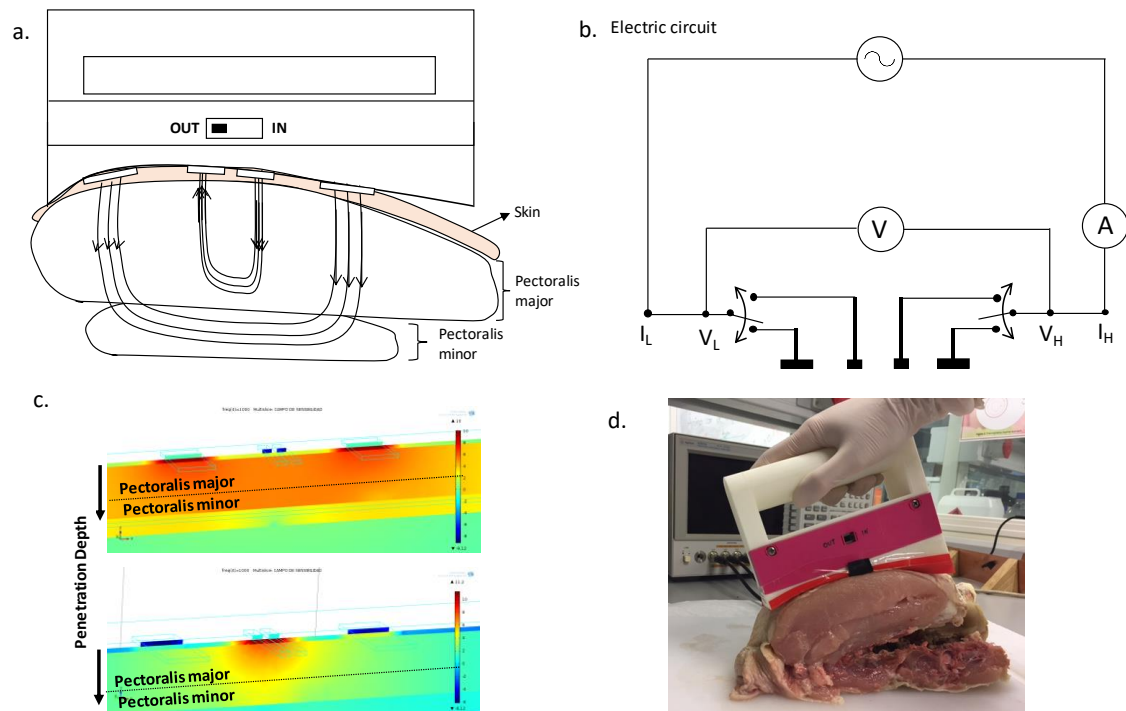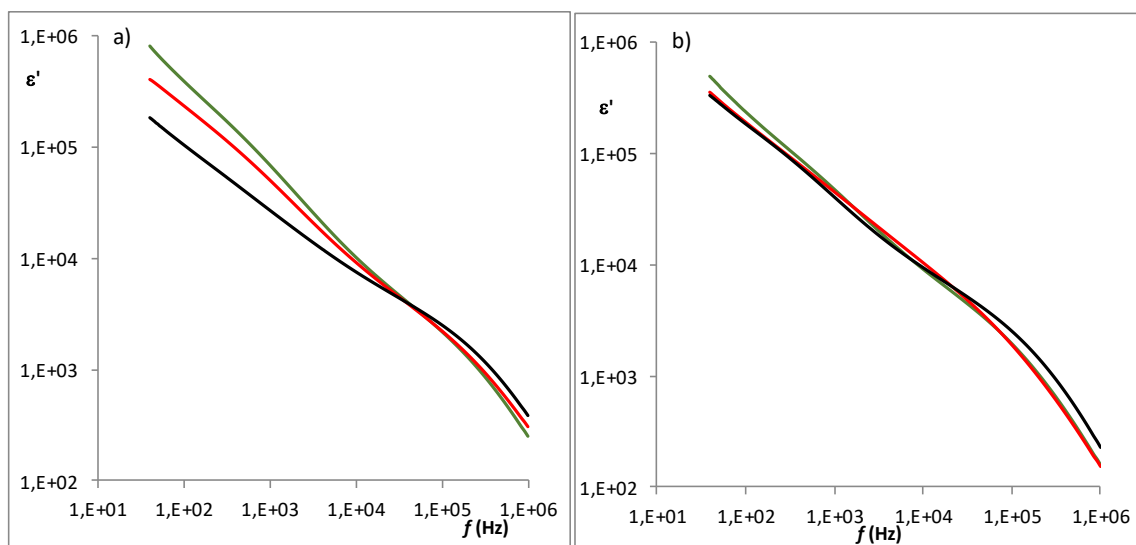**Figure 6**

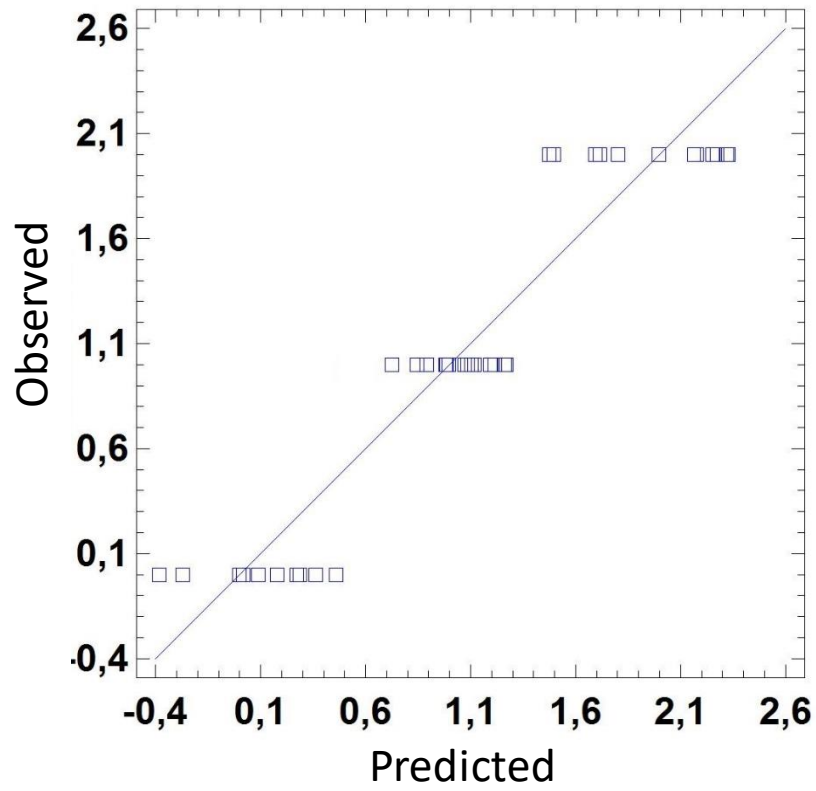**Figure 7**

Figure 7

Figure 8

Figure 8

Table 1

Table 1. Thermogram analysis of Pectoralis minor and major obtained by DSC. 0: normal, 1: hemorrhagic/hematoma and 2: necrotic muscles. Standard deviation values are included.

	Pectoralis minor			*Pectoralis major*		
Categories	Myosin (g_{prot}/g_T)	Collagen and Sarcoplasmic (g_{prot}/g_T)	Actin (g_{prot}/g_T)	Myosin (g_{prot}/g_T)	Collagen and Sarcoplasmic (g_{prot}/g_T)	Actin (g_{prot}/g_T)
0	0.10 ± 0.03^a	0.086 ± 0.01^a	0.05 ± 0.01^a	0.10 ± 0.02^a	0.086 ± 0.01^{ab}	0.05 ± 0.01^a
1	0.08 ± 0.05^{ab}	0.07 ± 0.03^{ab}	0.02 ± 0.02^b	0.10 ± 0.03^a	0.10 ± 0.03^a	0.03 ± 0.02^b
2	0.03 ± 0.01^b	0.05 ± 0.03^b	0.003 ± 0.003^b	0.06 ± 0.03^b	0.07 ± 0.02^b	0.04 ± 0.01^b

[a-b] Different letters on the columns indicate significant differences between means ($p < 0.05$).

Table 2

1

2

3   **Table 2.** Mass fraction of the most important cations (ppm) and lactate mass fraction

4   (ppm) of *Pectoralis minor* at 16 h of pmt for the different categories. pH of *Pectoralis*

5   *minor* and *major* at the same pmt.

	NORMAL			category 1			category 2		
Na^+	130	±	8	1580	±	28	868	±	63
K^+	353	±	27	1646	±	86	556	±	81
Ca^{2+}	190	±	43	342	±	69	213	±	69
Mg^{2+}	80	±	12	78	±	6	87	±	12
lactate$^-$	5519	±	64	4377	±	51	495	±	6
$pH_{pect.\ minor}$	5.87	±	0.06	6.11	±	0.07	7.04	±	0.11
$pH_{pect.\ major}$	5.8	±	0.2	5.9	±	0.2	5.9	±	0.2

6

7

8

9

FIGURE CAPTION

Figure 1. Micrographies of *Pectoralis minor* obtained by Cryo-SEM microscopy, where: a) normal muscle tissue, b) hemorrhagic with hematomas and blood clots and c) necrotic samples. Micrographies on the right 2000x and left 1000x.

Figure 2. Dielectric constant spectra of a) *Pectoralis major*, b) *Pectoralis minor*, where: (-) NORMAL tissue, (-) hemorrhagic samples with hematomas and blood clots and (-) necrotic samples.

Figure 3. Relation between the lactate content and the dielectric constant in the relaxation of α-dispersion, for each category at 16 h pmt.

Figure 4. Relation between the dielectric constant in the relaxation of β-dispersion with a) collagen and sarcoplasmic protein content (kg_c/kg_T) and b) myosin content (kg_m/kg_T), for each category at 16 h pmt.

Figure 5. Relation between the dielectric constant in the relaxation of γ-dispersion with the moisture (kg_w/kg_T) for each category at 16 h pmt.

Figure 6. Schematic representation of a. the signal penetration by using the flat plates at different distances, b. the electric circuit, c. corresponds to the COMSOL simulation of the signal penetration using each pair of flat plates and d. image of the developed sensor measuring a whole carcass. A: ampere meter; V: voltmeter; I_L: low current; I_H: high current; V_L: low voltage and V_H: high voltage. Spanish patent number: P201630062 (Fito et al., 2016).

Figure 7. Samples of dielectric constant spectra of a) IN Conformation, b) OUT Conformation, where: (-) NORMAL breast carcass, (-) carcass with hemorrhagic *pectoralis minor* and (-) carcass with necrotic *pectoralis minor*.

Figure 8. Predicted categories based on the developed algorithm versus the real categories.